sustainability

MDPI

Article

Simplified Analytical Model and Shaking Table Test Validation for Seismic Analysis of Mid-Rise Cold-Formed Steel Composite Shear Wall Building

Jihong Ye [1,*] and Liqiang Jiang [2]

[1] Jiangsu Key Laboratory Environmental Impact and Structural Safety in Engineering, China University of Mining and Technology, Xuzhou 211116, China

[2] School of Mechanics, Civil Engineering and Architecture, Northwestern Polytechnical University, Xi'an 710072, China; 230149388@seu.edu.cn

* Correspondence: jhye@cumt.edu.cn

Received: 10 August 2018; Accepted: 5 September 2018; Published: 6 September 2018

Abstract: To develop the cold-formed steel (CFS) building from low-rise to mid-rise, this paper proposes a new type of CFS composite shear wall building system. The continuous placed CFS concrete-filled tube (CFRST) column is used as the end stud, and the CFS-ALC wall casing concrete composite floor is used as the floor system. In order to predict the seismic behavior of this new structural system, a simplified analytical model is proposed in this paper, which includes the following. (1) A build-up section with "new material" is used to model the CFS tube and infilled concrete of CFRST columns; the section parameters are determined by the equivalent stiffness principle, and the "new material" is modeled by an elastic-perfect plastic model. (2) Two crossed nonlinear springs with hysteretic parameters are used to model a composite CFS shear wall; the Pinching04 material is used to input the hysteretic parameters for these springs, and two crossed rigid trusses are used to model the CFS beams. (3) A linear spring is used to model the uplift behavior of a hold-down connection, and the contribution of these connections for CFRST columns are considered and individually modeled. (4) The rigid diaphragm is used to model the composite floor system, and it is demonstrated by example analyses. Finally, a shaking table test is conducted on a five-story 1:2-scaled CFS composite shear wall building to valid the simplified model. The results are as follows. The errors on peak drift of the first story, the energy dissipation of the first story, the peak drift of the roof story, and the energy dissipation of the whole structure's displacement time–history curves between the test and simplified models are about 10%, and the largest one of these errors is 20.8%. Both the time–history drift curves and cumulative energy curves obtained from the simplified model accurately track the deformation and energy dissipation processes of the test model. Such comparisons demonstrate the accuracy and applicability of the simplified model, and the proposed simplified model would provide the basis for the theoretical analysis and seismic design of CFS composite shear wall systems.

Keywords: cold-formed steel structure; cold-formed steel composite shear wall building; mid-rise; simplified modeling method; seismic analysis; shaking table test

1. Introduction

Cold-formed steel (CFS) composite shear wall buildings are widely used around the world due to their advantages, such as: light weight, recyclable materials, high assembly, short construction time cycle, etc. Such buildings were commonly used in low-rise villas or apartments within three stories. In China, this type of building system has attracted increasing attention from structural engineers. However, researchers [1] believe that mid-rise CFS buildings would be more appropriate for Chinese

civil constructions, because China has insufficient land for its extensive people. In fact, the United States (US) National Science Foundation (NSF) and the American Iron and Steel Institute (AISI) funded the Cold-formed Steel-National Science Foundation Network for Earthquake Engineering Simulation (CFS-NEES) research project, and the main objective of the project is searching constructional technologies and perform-based seismic design methodologies for mid-rise CFS structures [2]. Thus, it can be seen that the technologies in mid-rise CFS structures are a common issue for the CFS researchers allover the world.

In the past three decades, researchers contributed lots of studies on the seismic performance and seismic design methods on low-rise CFS structures. Serrete et al. [3] discussed the CFS shear wall sheathed with different kinds of wallboard, including plywood, oriented strand board (OSB), gypsum, and fiberboard. Such works were adopted by the AISI S213 (AISI 2007). Then, Rogers et al. developed new types of CFS shear wall, such as a CFS wall with an X-shape strap [4] and a CFS steel-sheathed shear wall [5], and proposed two-stage modeling and seismic design methods for the steel-sheathed CFS shear walls [6]. Ronagh et al. [7] conducted experimental and numerical studies on the braced CFS shear walls. Yu et al. contributed several works on the seismic tests and design methods of steel-sheathed CFS shear walls [8]. Landolfo et al. [9–12] conducted cyclic tests on CFS wood-sheathed shear walls and fasteners, and CFS shear walls sheathed with nailed gypsum panels. Besides, Landolfo et al. tested a two-story CFS building to propose a perform-based seismic design method of CFS buildings [13,14]. Bourahla et al. [15,16] developed a deteriorating hysteresis model and seismic design procedure for CFS structures. Dubina et al. developed design methods for CFS walls sheathed with wood and gypsum [17], and generated a numerical model for seismic analysis for CFS buildings [18]. Schafer et al. conducted a shaking table test of a two-story full-scale CFS-framed office building, and discussed the system-level [19] and the subsystem-level [20] responses of the building. The modeling methodology on the test building was also proposed [21], and a reliability assessment was performed on the CFS buildings as well [22].

In addition to the research works on low-rise CFS structures, researchers have focused on realizing the construction of mid-rise CFS buildings through the following manners: (1) the hot-rolled section steel frame is proposed to be used as the main bearing component, and the CFS walls are filled in the steel frames; (2) new types of CFS shear walls with superior seismic performance are developed to satisfy the seismic demand of mid-rise CFS structures, such as a CFS shear wall sheathed with double-layer wallboards [23] and braced CFS shear walls [7]. Furthermore, various types of mid-rise CFS structural systems were also adopted by the structural engineers [2]. Ye et al. proposed a new type of CFS shear wall [24,25], in which the CFS concrete-filled steel tube (CFRST) was proposed as the end stud of the shear wall. Both a cyclic test and an analytical model were conducted to analyze the seismic performance and collapse mechanism of the proposed CFS shear walls [26–28]. The following researchers finished many experimental (including shaking table tests and cyclic tests), numerical, and theoretical works for the CFS structures, and many design guidelines were also adopted to design the CFS structures, such as AISI S400 (AISI 2015) [29]. However, as stated by Schafer [2], these works were mostly focusing on the component level; the system-level investigations of CFS structures are still insufficient, especially for the mid-rise CFS structures. The most effective way to understand the system-level responses of mid-rise CFS structures is developing shaking table tests and an accurate and reliable numerical modeling method for mid-rise CFS structures [2].

Therefore, this paper proposes a simplified numerical modeling methodology for the seismic analysis of mid-rise CFS structures based on a shaking table test of a 1:2 scaled five-story CFS composite shear wall building. The research steps can be summarized as follows. (1) In the second section of this paper, a brief introduction of the key construction technologies for the mid-rise CFS building system is made through comparison with the low-rise building system. (2) In the third section of this paper, the detailed modeling processes of the parts of the mid-rise building are described, including the CFRST columns, CFS composite shear walls, hold-down connections, and composite floor systems.

(3) In the fourth section of this paper, the results, including the natural frequency, structural drift, and cumulative energy obtained from the simplified model are validated by the test results.

2. A Five-Story Shaking Table Test Model

A 1:2 scaled five-story CFS composite shear wall building was designed and tested, as shown in Figure 1a. Such a building was designed according to the scale similarity. The prototype building was built in the a high seismic zone (eight-degree seismic fortification zone) in China, and it was designed according to the Chinese Code for the Seismic Design of Buildings GB 50011-2010 [30] and Chinese Technical Code of Cold-Formed Thin-Walled Steel Structures JGJ227-2011 [31]. The total height of the prototype building was 15 m, and it was 3 m for each story. The span was 3.6 m. The height of the scaled building was 7.5 m, and the span was 1.8 m. The scaled building was designed according to the geometrical, load, mass, stiffness, and initial condition similarities, and the scale similarity was shown in Table 1. The length and the width of the shaking table were 6 m and 4 m, respectively. Unidirectional earthquake was input by the Mechanical Testing System (MTS) actuator, and the layout of the test model on the shaking table is shown in Figure 1b. The bearing capacity of the shaking table is 25 t, and the maximum displacement of it is ±250 mm. The test model used the new scheme to realize the mid-rise construction, which was different from the low-rise construction scheme in the following two ways. (1) The continuous CFRST was used as end studs along the height, and the CFRST columns included "+"-shape inner columns, "T"-shape side columns, and "L"-shape corner columns, as shown in Figure 1b. (2) The CFS joists and the Autoclaved Lightweight Concrete (ALC) boards were used as a composite floor system, and the case-in-place concrete was placed on the composite floor to enhance the integrality of the floor system, as shown in Figure 2a. The details of the composite floor system, CFS studs placement, and the beam–column joints are shown in Figure 2.

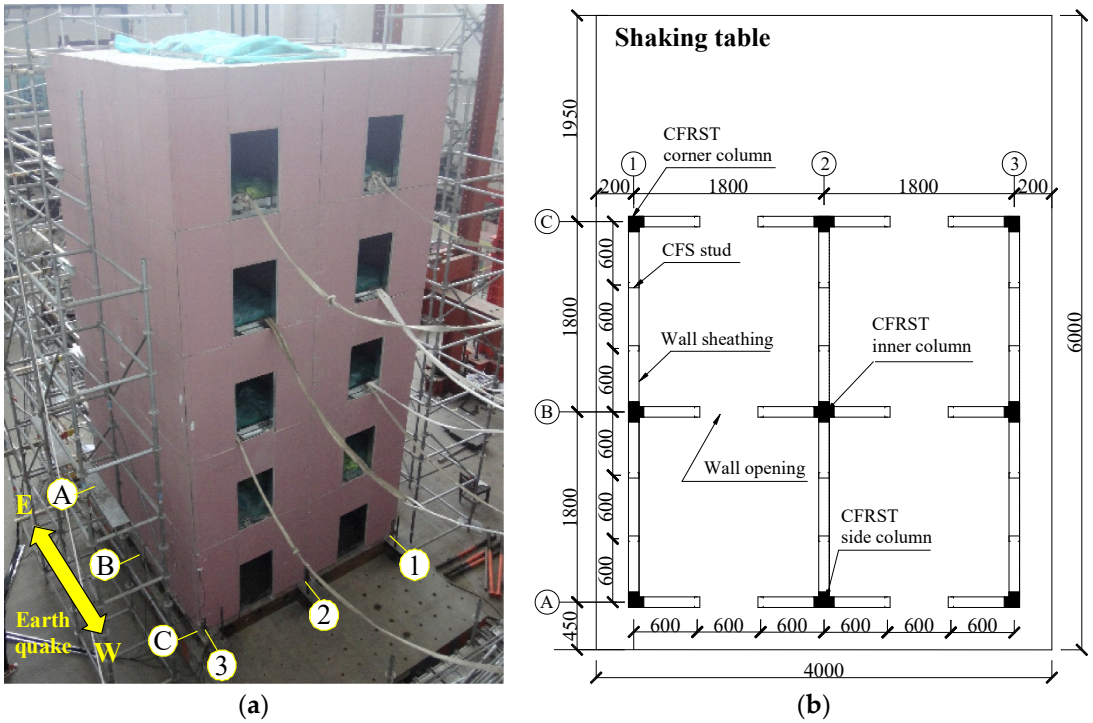

Figure 1. Layout and dimension of the test model. (**a**) Three-dimensional (3D) view; (**b**) Plan view.

The CFS composite shear walls used in the test model include the shear walls along the direction of earthquake (one-axial, two-axial, and three-axial), and the shear walls without earthquake input (A-axial, B-axial, and C-axial), as shown in Figures 1 and 2. All of the shear walls were sheathed with 12-mm gypsum wallboard at both sides, and were connected with the CFS frames through screws.

A 0.9-m height and 0.6-m width door opening was placed on each shear wall without earthquake input, as shown in Figure 1b. The CFS composite floor was placed between each story, and it included build-up I-shape CFS beams that were 150 mm in height (it is built by U150 × 50 × 0.8, unit: mm), 50-mm thick ALC boards, and a 30-mm thick concrete floor, as shown in Figure 2c. Two C89 studs (C89 × 50 × 13 × 0.8, unit: mm) were included in each shear wall, and the distance of these studs was 600 mm, as shown in Figure 1b. Hold-downs were placed at the ends of the CFRST columns, and the height of them was 270 mm. Such hold-downs were connected with the CFRST columns through screws.

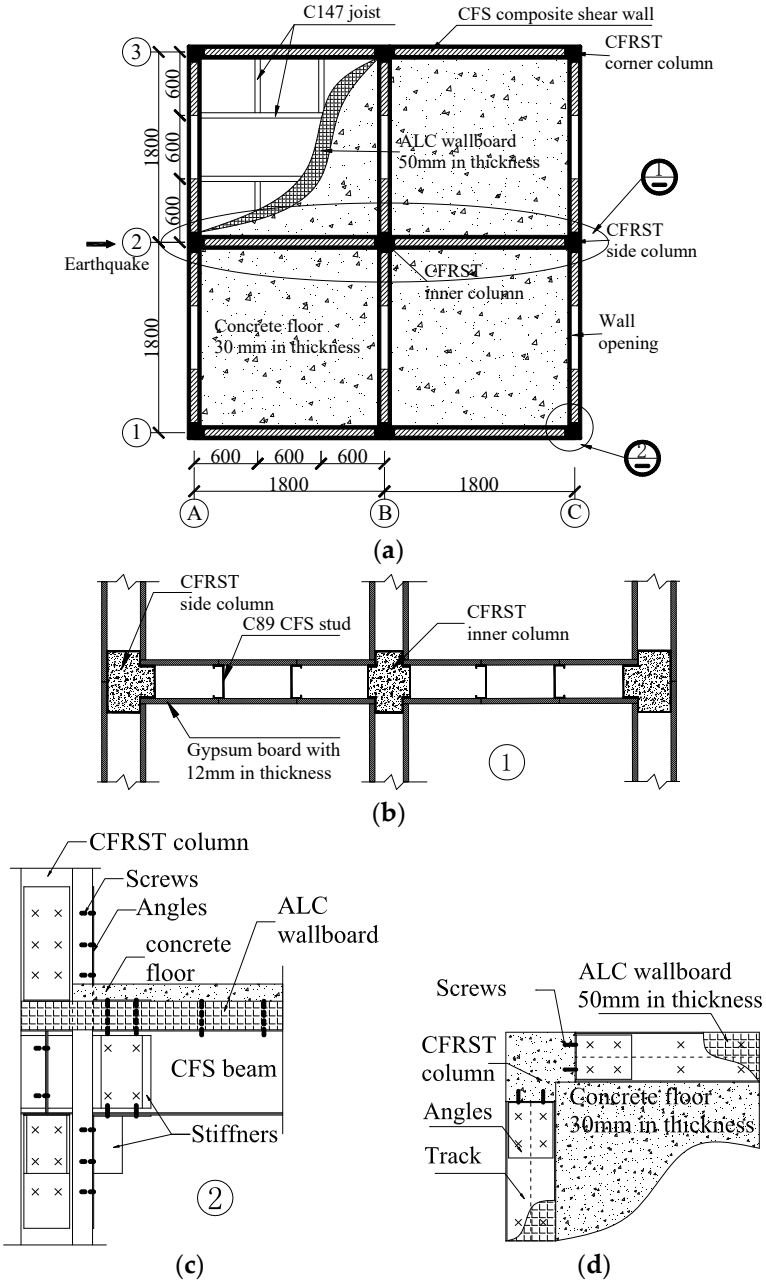

Figure 2. Details of the floor, shear wall, and beam–column joint (Unit: mm). (**a**) Layout of the floor system; (**b**) Layout of the partial shear wall ①; (**c**) Elevation of the corner column joint ②; (**d**) Planar of the corner column joint ②.

In total, five displacement sensors and five acceleration sensors were placed on each story to measure the lateral displacement and acceleration of the test model subject to the earthquake, as shown

in Figure 3. The El Centro earthquake along the north–south direction was used as the prototype earthquake, as shown in Figure 4. The earthquakes were input on the test model consequently according to the peak acceleration on a multiple of 100 gal, and the vibration results of the test model were recorded.

Table 1. Scale similarity between the prototype and the test models.

Items	Parameters	Symbols	Similarity Factors
Geometric parameters	Length	S_L	1/2
	Area	S_A	1/4
	Drift ratio	S_α	1
Material parameters	Strain	S_ε	1
	Elastic modulus	S_E	1
	Stress	S_σ	1
	Poisson's ratio	S_μ	1
	Mass density	S_ρ	2
Load parameters	Concentrated force	S_P	1/4
	Area load	S_q	1
Dynamic parameters	Period	S_T	$1/\sqrt{2}$
	Frequency	S_f	$\sqrt{2}$
	Acceleration	S_a	1
	Gravity acceleration	S_g	1
	Damping ratio	S_C	$1/2^{1.5}$

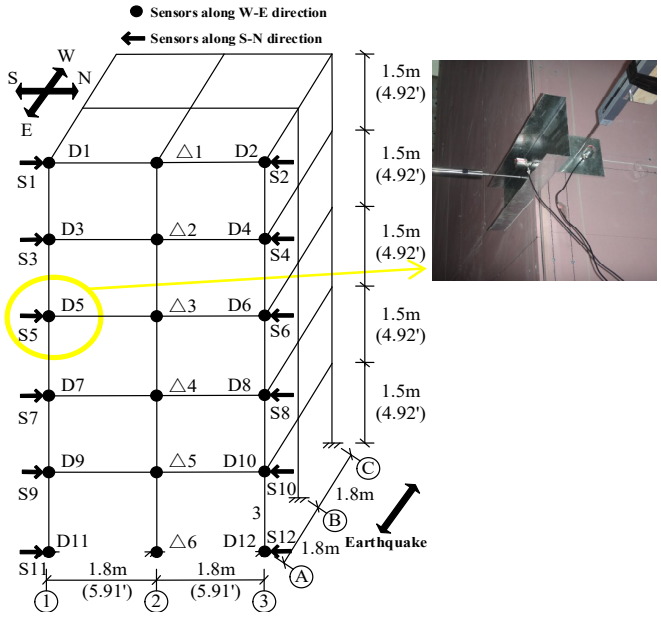

Figure 3. Measurements of the shaking table test model.

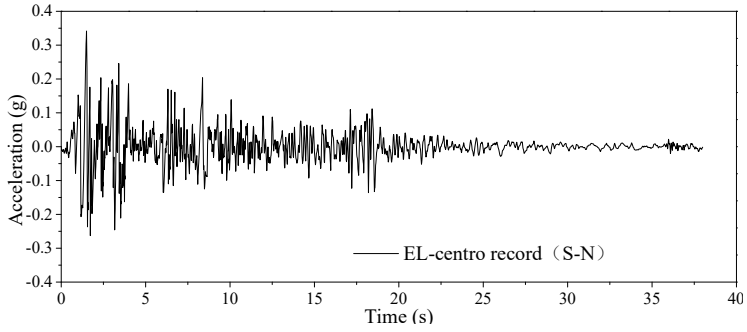

Figure 4. Prototype earthquake record of the shaking table test (El Centro in S–N direction).

3. Simplified Analytical Model of the Test Specimen

The simplified analytical model of the test specimen is presented in Figure 5. Since the two-axial is the symmetry axial for the test model, only the simplified models for the one-axial and two-axial shear walls are shown in Figure 5. Such simplified models are realized by the *Open System of Earthquake Engineering Simulation* software OpenSees [32]. The simplified model follows the following estimations.

(1) A build-up section beam is idealized as two crossed rigid links, and such links are pinned with CFRST columns. The CFS composite floor system is idealized as a rigid plane, and the rigid plane is pinned with the CFRST columns.

(2) A CFS composite shear wall (including the sheathing wallboards and the CFS studs) is idealized as two crossed nonlinear springs, and the hysteretic characteristics of the composite shear wall are represented by the nonlinear springs.

(3) The hold-down connections at the ends of the CFRST columns are idealized as rigid connections, and the uplift behavior of the hold-down connections is modeled by an axial linear spring according to suggestions of previous study [26]. Thus, in the simplified model, three rotational freedoms and two translation freedoms are restrained, and the axial translation freedom is restrained by the axial linear spring.

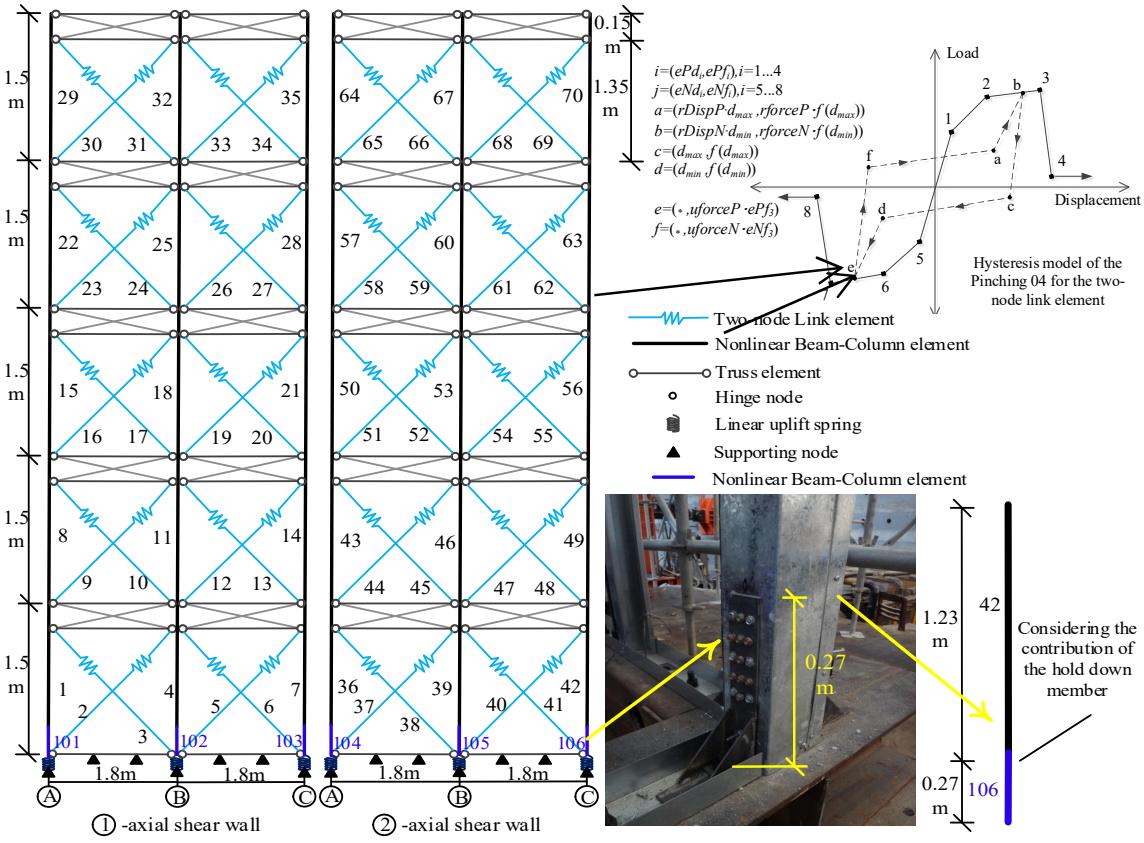

Figure 5. Simplified analytical model for the shaking table test specimen.

3.1. Modeling the CFRST Column

According to the failure modes of the shaking table test model, the CFRST columns buckled under the combination of gravity loads and earthquakes; thus, the nonlinear behavior of the CFRST columns should be considered in the simplified model. In previous studies, the end studs were simplified as a linear truss [6], or a CFRST column was simplified as a linear beam–column element and a linear spring [26]. However, such simplifications cannot capture the nonlinear behavior of the

CFRST columns. Padilla-Llano [33] proposed a complete nonlinear hysteretic model for each CFS stud; however, as stated by Leng et al. [21], such a model would result in excessive computational cost or computational non-convergence. Therefore, this paper simplifies the CFRST columns as a build-up section with "new material", and the columns are modeled by the nonlinear beam–column elements of OpenSees. The material properties of the build-up section are listed in Table 2 according to the mechanical interaction between the CFS and infilled concrete, including axial force, moment, and torque.

Table 2. Definition of the cold-formed steel (CFS) concrete-filled tube (CFRST) column in the simplified model.

Items	Constitutive	Stiffness	Load Capacity
Axial force	Elastic-perfect plastic	EA	P
Strong axis moment	Elastic-perfect plastic	EI_x	M_{nx}
Weak axial moment	Elastic-perfect plastic	EI_y	M_{ny}
Torque	Elastic	GJ	∞

The section parameters of the build-up section are determined according to the equivalent bending stiffness of the CFRST columns, the resistance of which is determined according to the American Institute of Steel Construction- Load and Resistance Factor Design (AISC-LRFD) [34,35]:

$$\begin{aligned} &N_{\mathrm{AISC}} = A_{\mathrm{s}}(0.658^{\lambda_{\mathrm{c}}^2})F_{\mathrm{my}};\ \lambda_{\mathrm{c}} = \frac{kL}{\pi}\sqrt{\frac{F_{\mathrm{my}}}{E_{\mathrm{m}}}};\\ &F_{\mathrm{my}} = f_{\mathrm{y}} + 0.85f'_{\mathrm{c}}(A_{\mathrm{c}}/A_{\mathrm{s}});\ E_{\mathrm{m}} = E_{\mathrm{s}} + 0.4E_{\mathrm{c}}(A_{\mathrm{c}}/A_{\mathrm{s}}) \end{aligned} \tag{1}$$

where E_{s}, E_{c}, and E_{m} are the elastic modulus for the CFS members, the infilled concrete, and the "new material", respectively; A_{s} and A_{c} are the area of the CFS members and concrete in CFRST columns, respectively; f_{y} and f_{c} are the yield strength and compressive strength of the CFS and concrete, respectively; and N_{AISC} is the axial compressive capacity of the CFRST columns. Since the elastic-perfect plastic model is used for the build-up section in the cases of axial force and moment, thus, the yield strength of the "new material" is simplified as $N_{\mathrm{AISC}}/A_{\mathrm{e}}$, where A_{e} is the area of the build-up section.

Due to the CFRST columns being designed as "+"-shape, "T"-shape, and "L"-shape sections for the test model, as shown in Figure 6, it is thus necessary to calculate the section and material parameters for them; the results are shown in Table 3. In Table 3, the bottom region of the CFRST columns is the region considering the contribution of the hold-down members, which can be seen in Figure 5. In the simplified model, the contributions on bending stiffness and axial compressive stiffness of the hold-down members are considered; such regions are individually modeled, and the section and material parameters of these regions are listed in Table 3.

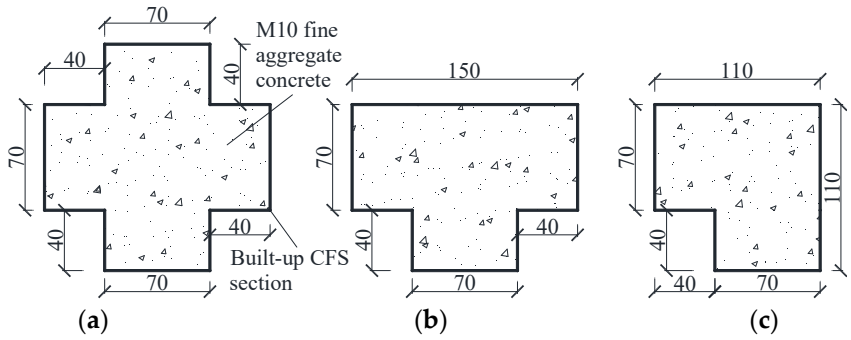

Figure 6. Section of the CFRST columns (unit: mm, thickness of CFS members is 0.8 mm). (**a**) Inner column; (**b**) Side column; (**c**) Corner column.

Table 3. Parameters of the simplified model for the CFRST columns in the test specimen.

Items		Middle Region of the Column				Bottom Region of the Column		
		E_m/MPa	A_e/mm^2	f_{ey}/MPa	I_{ex}/mm^4	E_m/MPa	A_{es}/mm^2	I_{esx}/mm^4
Inner column		4.26×10^5	565.7	411.1	1.27×10^6	4.26×10^5	952.6	2.74×10^6
Side column	Strong axial	3.92×10^5	528.1	369.3	1.04×10^6	3.92×10^5	818.3	2.63×10^6
	Weak axial	3.92×10^5	528.1	383.0	1.30×10^6	3.92×10^5	818.3	2.24×10^6
Corner column		3.76×10^5	473.4	324.5	0.73×10^6	3.76×10^5	666.7	1.71×10^6

Note: E_m, A_e, f_{ey}, and I_{ex} are the elastic modulus, area, yield strength, and inertia moment along the direction of the earthquake, respectively; the bottom region of the column is the region strengthened by the hold-down (the height is 270 mm, as shown in Figure 5); A_{es}, f_{esy}, and I_{esx} are the equivalent area, yield strength, and inertia moment of the CFRST column at the strengthened region.

3.2. Modeling the CFS Composite Shear Wall

The CFS composite shear wall includes build-up I-shape CFS beams, gypsum wallboards, and CFS studs. Two crossed rigid trusses are used to model a build-up I-shape CFS beam, because no obvious damage and deformation were observed on these CFS beams, according to the shaking table test. Two crossed two-node link elements are used to model the nonlinear behavior of a composite shear wall, and Pinching04 material is used to represent the hysteretic behavior of these two-node link elements. The hysteretic parameters for the Pinching04 material are always determined from the cyclic test results of the prototype CFS composite shear walls. As the composite shear wall is simplified as two crossed elements; thus, the relation between the load–displacement curve of the shear wall and the load–displacement curve of the simplified element is following the geometric relationship, which is also presented in Figure 7:

$$F' = F/2\cos\theta \tag{2}$$

$$\Delta'_w = \Delta_w \cdot \cos\theta \tag{3}$$

where θ is the angle between the simplified element and the top track of the shear wall; F and Δ_w are the load and the displacement of the shear wall, respectively; and F' and Δ'_w are the load and the displacement of the simplified element, respectively.

However, there is not cyclic test data for the 1:2 scaled CFS composite shear wall constructed in the test model of this paper. Thus, this paper determines the hysteretic parameters for the scaled composite shear wall according to the fastener-based model, as shown in Figure 8a; such a model was proposed by the CFS-NESS team [36]. In the fastener-based model, the wallboard is estimated as a rigid plane, a screw is idealized as a nonlinear spring with hysteretic parameters, and the hysteretic parameters are obtained from the cyclic tests on fasteners. Such a model was verified by cyclic test results [21]; the authors' research team validated such a model through cyclic tests on single-story and double-story CFS composite shear walls [26], and the results of specimen W1 are depicted in Figure 8b. Such a model can be realized by the following steps.

(1) Based on the fastener-based model, the hysteretic curves for the target CFS composite shear walls can be obtained. (2) The hysteretic parameters for the target shear wall can be obtained from the hysteretic curves, as shown in Figure 9. (3) The hysteretic parameters of the nonlinear springs for the target shear wall can be determined according to Equations (1) and (2), and such parameters can be used in the simplified model. Thus, the hysteretic parameters for the composite shear walls that are used in the test model are listed in Table 4.

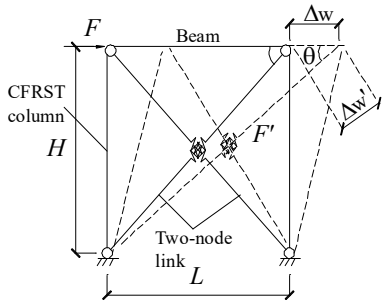

Figure 7. Mechanical and deformation diagrams of the shear wall subject to the horizontal load.

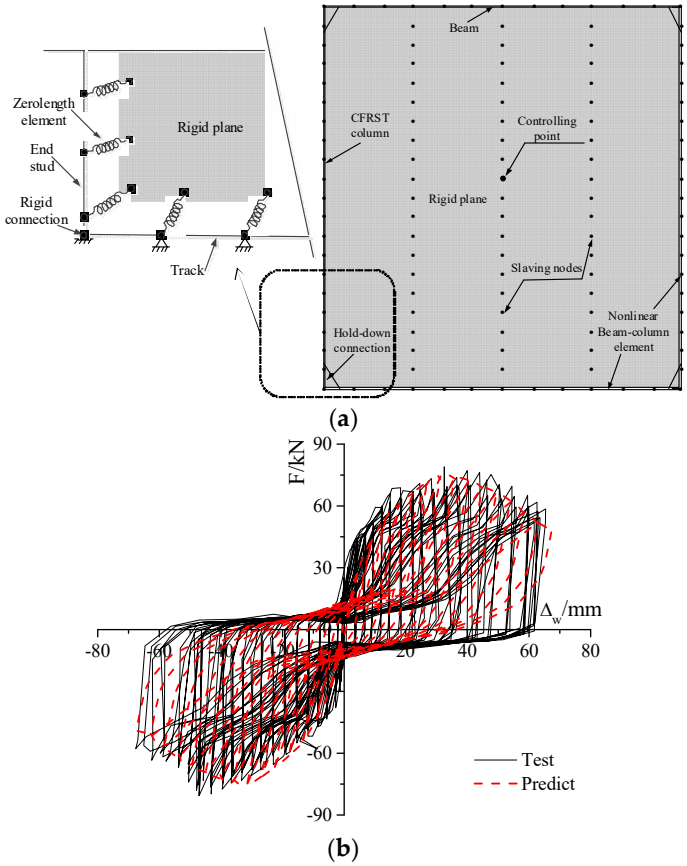

Figure 8. Test validation of the fastener-based model for numerical analysis of the shear wall. (**a**) Fastener-based model; (**b**) Test validation.

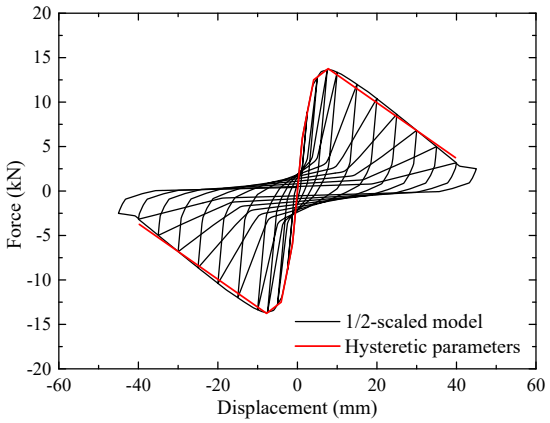

Figure 9. Hysteretic parameter determination of the half-scaled shear wall.

Table 4. Hysteretic parameters of the shear walls in the simplified model for the test specimen.

	Hysteretic Parameters of Shear Walls											
	Item	epd_i/mm i = 1–4	epf_i/kN i = 1–4	*rDispP*	*rforceP*	*uforceP*	a_{Klimit} = 0.5		a_{Dlimit} = 0.2		a_{Flimit} = 0.05	
							$a_{K1,2}$	$a_{K3,4}$	$a_{D1,2}$	$a_{D3,4}$	$a_{F1,2}$	$a_{F3,4}$
Equivalent members of the shear walls	Axial of 1, 2, 3	1.96, 4.15, 8.95, 50.52	5.88, 8.14, 9.96, 2.44	0.3	0.3	0.05	0.5	1.5	0.4	1.5	0.4	1.5
	Axial of A, B, C	1.67, 5.02, 10.56, 45.30	4.23, 5.68, 7.84, 2.79	0.3	0.3	0.05	0.5	1.5	0.4	1.5	0.4	1.5

Note: epd_1–epd_4, epf_1–epf_4, *rDispP*, *rforceP*, and *uforceP* are the hysteretic parameters of the shear walls, as shown in Figure 5; a_{Klimit}, a_{Dlimit}, and a_{Flimit} are the damage factors to describe the hysteretic characteristics of the shear walls, which can be determined by the stiffness and strength of the loading and unloading stages for the Pinching04 model in Figure 5.

3.3. Modeling the Hold-Down Connections

Due to the restraining effects of hold-down connections on CFRST columns, the uplift behavior might occur on these connections [6,21,26]. Thus, the deformation of the uplift behavior should be considered in the simplified model. According to the shaking table test results, there were not obvious damages and deformation observed on the hold-down connections; thus, such connections were estimated as working in an elastic stage according the suggestions of cyclic tests on composite shear walls by the authors' research team [26]. Therefore, a linear spring is used to model the uplift behavior of a hold-down connection, according to the suggestions of Shamim and Rogers [6] and Wang et al. [26], and such a spring considers the tensile deformation, but does not consider the compressive deformation.

Due to the same size and same type of hold-down connection being used in the shaking table test model of this paper and the cyclic test model W89 shear wall of the authors' previous study [26], the stiffness of the linear spring was 39.2 kN/mm for two hold-down connections. In the shaking table test model, two, three, and four hold-down connections were used for the corner column, side column, and inner column, respectively. Thus, the stiffness of these springs is k_{corner} = 39.2 kN/mm, k_{side} = 58.8 kN/mm, and k_{mid} = 78.4 kN/mm for the corner column, side column, and inner column, respectively.

3.4. Modeling the Composite Floor System

Leng et al. [21] proposed rigid and semi-rigid diaphragm models for the composite floor system in the three-dimensional (3D) numerical model. The semi-rigid diaphragm model determined the shear deformation response by using engineering judgment, and it was found that the semi-rigid diaphragm was more appropriate for the CFS composite floor system. However, a new ALC wallboard CFS composite floor system is proposed and used for the shaking table test model by Ye et al. [37], as shown in Figure 2. The new floor system is different from the one used by Leng et al. [21]: the CFS joists and ALC wallboard (thickness of 50 mm to 100 mm) are used as the composite floor, and the cast-in-place concrete (thickness of 30 mm to 50 mm) is then poured on the composite floor to enhance its integrality. Among the load-carrying capacity, stiffness, fire resistance, and integrality would be effectively improved for the covering of the ALC wallboard and cast concrete [37].

Due to the complicate calculating processes and the engineering-based judgment of the semi-rigid diaphragm model proposed by Leng et al. [21], this paper adopts the rigid diaphragm model in the simplified model for the new composite floor system. To valid the simplified model, both semi-rigid and rigid diaphragm models are used to analyze the roof displacement time–history curves of the shaking table test model in the cases of 200 gal and 800 gal. In the simplified model, the RigidPlane element is used for the rigid diaphragm model, and crossed truss elements are used for the semi-rigid diaphragm model, according to the principle of equivalent stiffness. The results are shown in Figure 10, which demonstrate that the roof displacement time–history curves for rigid diaphragm model and semi-rigid diaphragm model closely resemble both the 200-gal case and the 800-gal case. Therefore,

the rigid diaphragm model is used to model the new composite floor system in the shaking table test model.

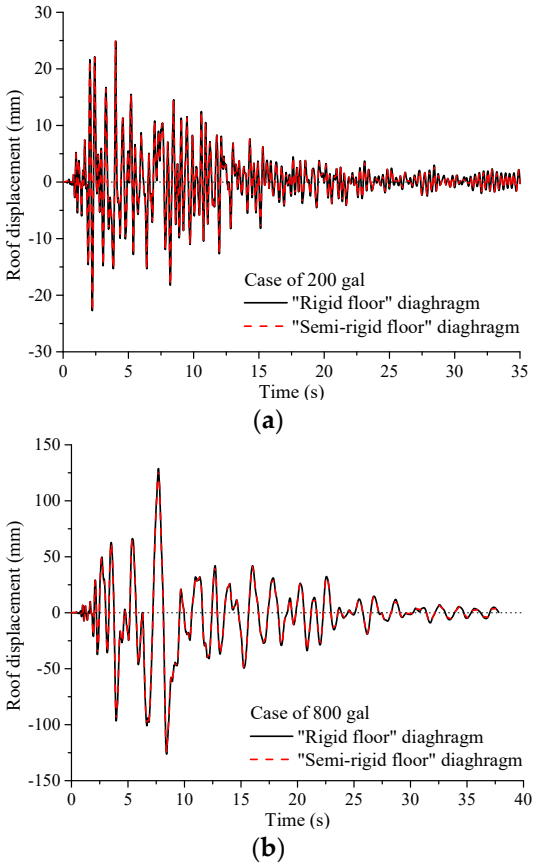

Figure 10. Comparison of roof displacement time–history curves between "Rigid floor" and "Semi-rigid floor" diaphragms. (**a**) Case of 200 gal; (**b**) Case of 800 gal.

3.5. Mass and Damping Ratio of the Building

The mass of a story is directly input on the rigid plane of this story, and it would be evenly distributed to the floor, CFRST columns, and studs through the rigid plane. The mass of a story includes the parts of the composite floor, half of the CFS shear walls and CFRST columns in the upper and lower stories, and the additional mass for modeling the live loads. The mass is 3753 kg and 1362 kg for the standard floor (first story to fourth story) and roof story (fifth story), respectively. Besides, the P-delta effect is also considered in the simplified model. Firstly, nine individual regions are divided for the floor according to the action area of the nine CFRST columns, and the gravity load of each region is input on the joint between the floor and the CFRST column corresponding to the region. The gravity load is directly input on the intersecting joint, and the position of the gravity load would be changed following the lateral deformation of the joint of the CFRST column due to the earthquake. Therefore, the P-delta effect can be considered in the simplified model.

The Rayleigh damping ratio is used in the simplified model. Shamim and Rogers [6] stated that the Rayleigh damping ratio showed significant influence of the numerical results for the CFS buildings, and that a 4% to 5% damping ratio was suitable for the CFS building through trial calculation. It was also found that such a value was larger than the commonly used value of steel structures (2% damping ratio), because the friction behavior would occur in the fabricated screw connections in the shear walls and the high-strength bolt connections at the column bases, and such behavior would increase the damping ratio of the CFS buildings. In the meanwhile, a 5% damping ratio was also proposed by Leng et al. [21] for CFS buildings, and the shaking table test results on a two-story full-scale CFS

building were used to valid the value of the damping ratio. Therefore, the Rayleigh damping ratio of 5% is used in the simplified model of this paper.

4. Validation of Simplified Models by Shaking Table Test

To validate the simplified analytical model, a five-story CFS 1:2 scaled composite shear wall building was tested and compared with the analytical results. Due to the relative slight residual deformation (less than 0.5 times of the value of maximum drift) of the test model that was subjected to different earthquake cases, the numerical analysis is individually proceeded for each earthquake case (including 300 gal, 500 gal, and 800 gal cases, which are used to valid the simplified models) according to the similar founding in the two-story full-scaled shaking test model by Peterman et al. [17,18].

To start with, white noise analysis with 100-gal peak acceleration was performed to obtain the natural frequency of the test model, which was 4.98 HZ along the earthquake direction. The first natural frequency of the simplified analytical model was 5.07 HZ along the same direction, and the error between the test and analytical models was 1.8%. The reason for the error can be concluded as: the boundary condition at the column base is considered as a rigid connection in the simplified model, and such an estimation would overestimate the lateral stiffness of the test model; thus, the natural frequency of the analytical model is larger than the value of the test model.

Figures 11–13 show the comparisons on first-story displacement time–history curves, the energy dissipation of the shear wall in the first story, the roof displacement time–history curves, and energy dissipation of whole structure between the shaking table test and analytical results corresponding to the 300-gal, 500-gal, and 800-gal cases, respectively. It can be seen that the simplified analytical model captures the dynamic responses of the shaking table model, and predicts the time–history processes and energy dissipation of the test model within different earthquake cases effectively. Such comparisons demonstrate the validity of the proposed simplified analytical model. By comparing the test and analytical results in the 300-gal, 500-gal, and 800-gal cases, the error among the peak drift of the first story, cumulative energy of the first story, the peak drift of the roof story, and the cumulative energy of the whole structure are no more than 20.8%, and most of the errors are about 10%, as shown in Table 5. Such comparisons are also demonstrating the high precision of the simplified analytical model.

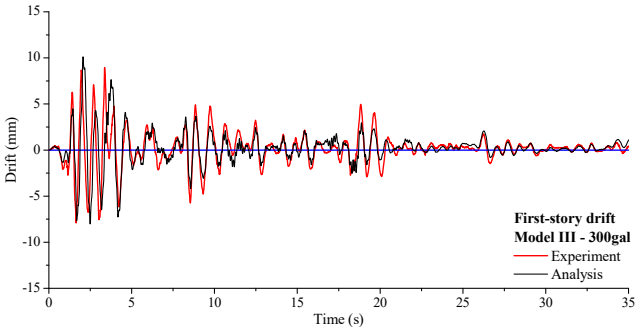

(**a**)

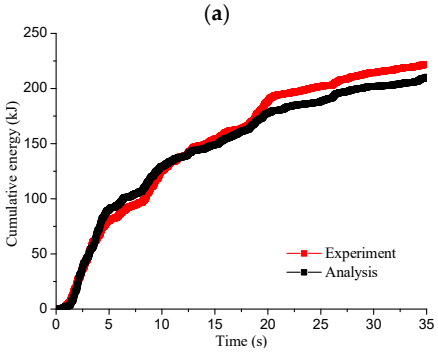

(**b**)

Figure 11. *Cont.*

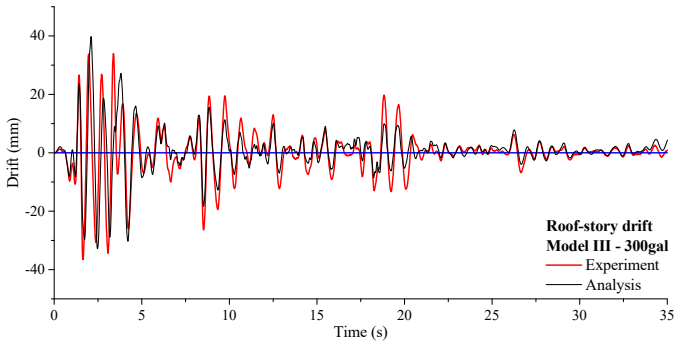

(**c**)

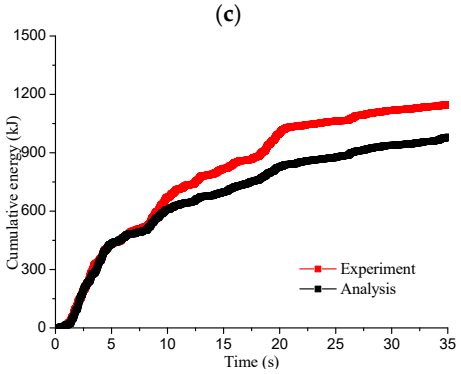

(**d**)

Figure 11. Comparison of time–history curves and cumulative energy between the test and numerical results in the case of 300 gal. (**a**) Story drift of the first story; (**b**) Cumulative energy of shear walls in the first story; (**c**) Roof drift; (**d**) Cumulative energy of the whole structure.

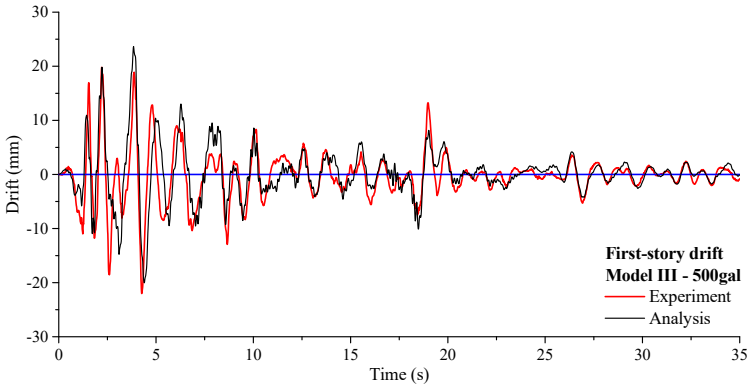

(**a**)

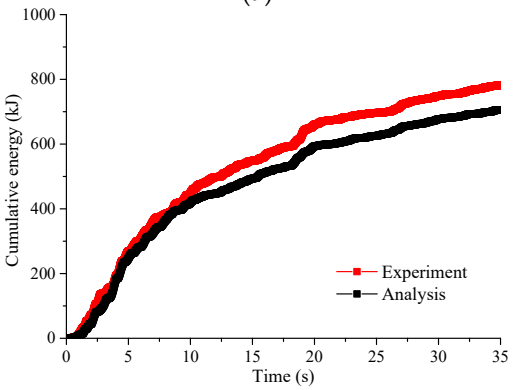

(**b**)

Figure 12. *Cont*.

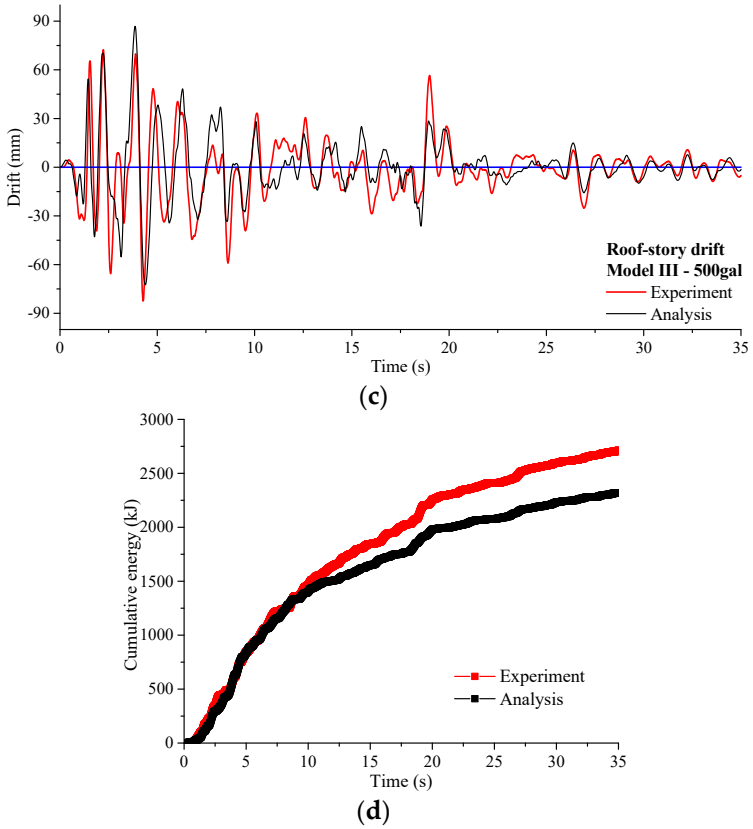

Figure 12. Comparison of time–history curves and cumulative energy between the test and numerical results in the 500-gal case. (**a**) Story drift of the first story; (**b**) Cumulative energy of the shear walls in the first story; (**c**) Roof drift; (**d**) Cumulative energy of the whole structure.

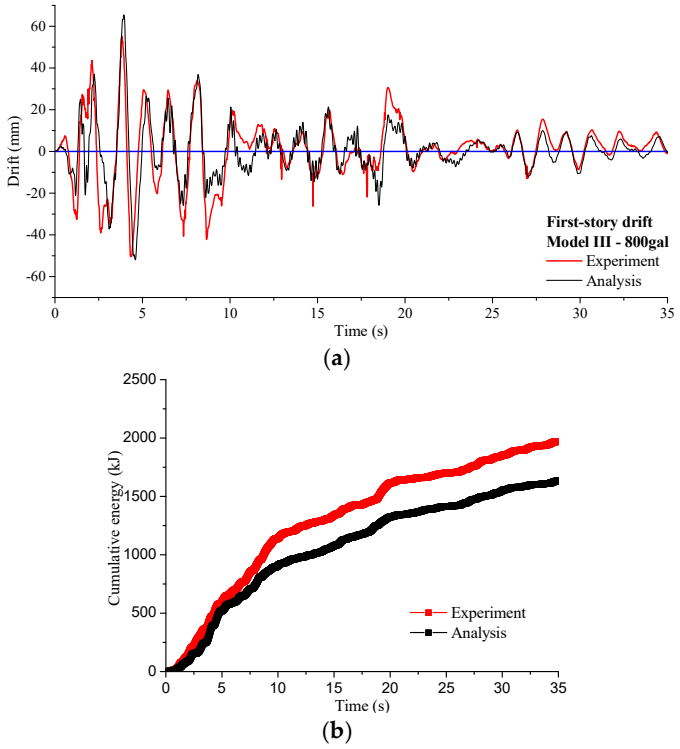

Figure 13. *Cont.*

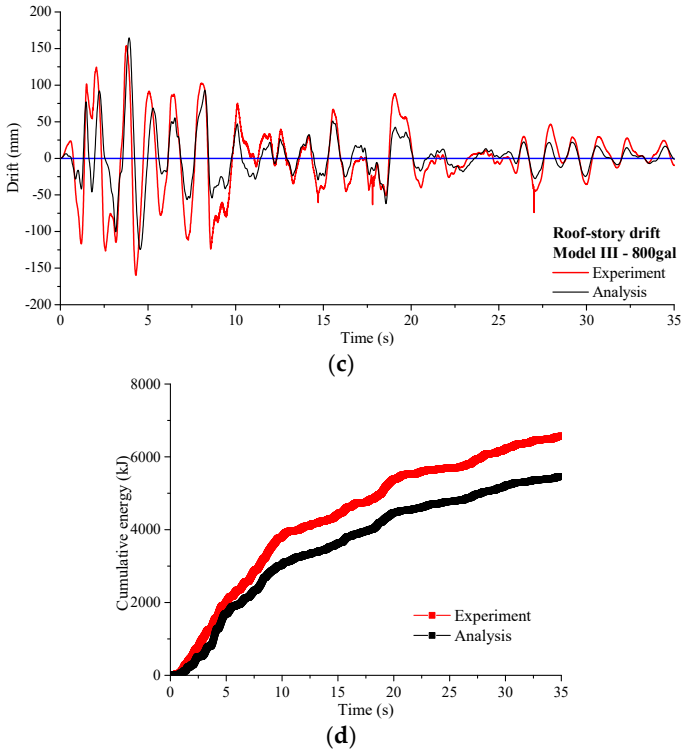

Figure 13. Comparison of time–history curves and cumulative energy between the test and numerical results in the 800-gal case. (**a**) Story drift of the first story; (**b**) Cumulative energy of shear walls in the first story; (**c**) Roof drift; (**d**) Cumulative energy of the whole structure.

Table 5. Comparison of the results between the test and numerical analysis.

Cases	Items	Maximum Drift of the First Story (mm)	Cumulative Energy of the Shear Wall in the First Story (kJ)	Maximum Roof Drift (mm)	Cumulative Energy of the Whole Structure (kJ)
300 gal	Test	8.98	221.72	36.76	1146.33
	Analysis	10.09	210.15	39.65	981.60
	Error	12.3%	5.2%	7.9%	14.4%
500 gal	Test	22.20	783.43	82.09	2703.41
	Analysis	23.52	705.19	86.35	2317.30
	Error	5.9%	10.0%	5.2%	14.3%
800 gal	Test	55.66	1969.88	165.05	6559.92
	Analysis	65.41	1631.09	153.47	5457.08
	Error	17.5%	20.8%	7.0%	16.8%

Note: The maximum acceleration of the output record from the shaking table is 305 gal, 514 gal, and 821 gal for the 300-gal, 500-gal, and 800-gal cases, respectively.

From Figures 11–13, it can be found that the cumulative energies both of the first story and the whole structure of the test model are larger than the analytical model, and the distance increases with the increasing peak acceleration of the earthquake. The reason can be drawn as follows. (1) The analytical model underestimates the energy dissipation of the structure, because the Pingching04 hysteretic model stipulated that the unloading stiffness was lower than the loading stiffness, but the unloading stiffness of the test shear wall was larger than the loading stiffness, as shown in Figure 8b (the opposition friction force derived from the pretension force of the screws between the CFS studs and gypsum wallboard). (2) The connections between the CFS beams and CFRST columns are idealized as pin connections in the analytical model; thus, the energy dissipation of these connections cannot be considered. Furthermore, both the peak drift of the first story and the peak drift of the roof story of the analytical results are larger than the values of the test, and the errors between them are not related to the peak acceleration of earthquake. Since the bond curve of the Pinching04

hysteretic model is divided into four segments, thus, the consecutive degradation relationship of the stiffness and strength of the composite shear walls is simplified as piecewise functions. This is the reason why there is an error between the tested and analyzed results.

5. Conclusions

This paper proposes a simplified analytical numerical model for the seismic analysis of mid-rise CFS composite shear wall building systems. The simplified model considers the mechanical behaviors of CFRST columns, composite CFS shear walls, hold-down connections, and composite floor systems, and detailed modeling methods are described for this simplified model. Finally, shaking table test results on a five-story 1:2-scaled CFS composite shear wall building are used to valid the simplified model, and the following conclusions are drawn:

1. The nonlinear mechanical behavior of the CFRST columns is considered in the simplified model, including the bucking behavior and the yielding of materials. A build-up section with "new material" is proposed to model the CFS tube and infilled concrete, and the equivalent stiffness principle is used to determine the section parameters. The material property of the "new material" is modeled by an elastic-perfect plastic model, and the equivalent yield strength is determined by AISC-LRFD guidance. Besides, the contribution of the hold-down connections on the lateral stiffness and axial strength of the column base of the CFRST columns is also considered in the simplified model, and the strengthened region (270 mm in height) is separately modeled with the CFRST column. Among the "+"-shape inner CFRST columns, the "T"-shape side CFRST columns, and the "L"-shape corner CFRST columns, their strengthened regions are modeled individually in the simplified model.
2. Two crossed nonlinear springs with hysteretic parameters are used in the simplified model to model the hysteretic behavior of a composite CFS shear wall subjected to earthquakes, and such behaviors are modeled by Pinching04 material. Two crossed rigid trusses are used to model a CFS beam. The fastener-based modeling method is used to determine the hysteretic parameters of the 1:2-scaled composite shear walls due to no cyclic test data for them.
3. A linear spring is used to model the uplift behavior of a hold-down connection in the simplified model, and the stiffness of this linear spring is determined by the cyclic test results of the composite shear walls. The stiffness of this linear spring is determined according to the numbers of hold-down connections for the CFRST inner columns, side columns, and corner columns, respectively.
4. To improve the computational efficiency of the simplified model, the rigid diaphragm method is used to model the composite floor system, and such a method is demonstrated by example analyses.

To sum up, the simplified model of the shaking table test model is built by OpenSees software, according to the above methodologies. By comparing the peak drift of the first story, the energy dissipation of the first story, the peak drift of the roof story, and the energy dissipation of the whole structure of the displacement curves between the simplified model and the test model, it is found that the errors between them are about 10%, and the largest one of these errors is 20.8%. It is also found that the rules of change of the time–history curves and cumulative energy curves obtained from the simplified model align closely with the measured results of the test model. The simplified model accurately tracks the whole deformation and energy dissipation processes of the test model. These demonstrations indicate that the simplified model exhibits high computational accuracy. Such works provide the basis for the theoretical analysis and seismic design of mid-rise CFS composite shear wall buildings.

Author Contributions: All authors contribute equally to this paper.

Acknowledgments: This research is sponsored by the National Key Program Foundation of China (51538002) and the Priority Academic Program Development of Jiangsu Higher Education Institutions, Scientific Innovation Research Foundation of Jiangsu, China (KYLX15_0090).

Conflicts of Interest: The authors declare no conflict of interest.

References

1. Ye, J.H. An introduction of mid-rise thin-walled steel structures: Research progress on cold-formed steel-framed composite shear wall systems. *J. Harbin Inst. Technol.* **2016**, *48*, 1–9.
2. Schafer, B.W.; Ayhan, D.; Leng, J.; Liu, P.; Padilla-Llano, D.; Perterman, K.D.; Stehman, M.; Buonopane, S.G.; Eatherton, M.; Madsen, R.; et al. Seismic responses and engineering of cold-formed steel framed building. *Structures* **2016**, *8*, 197–212. [CrossRef]
3. Serrette, R.; Encalada, J.; Juadines, M.; Nguyen, H. Static racking behavior of plywood, OSB, gypsum, and fiberboard walls with metal framing. *J. Struct. Eng.* **1997**, *123*, 1079–1086. [CrossRef]
4. Al-Kharat, M.; Rogers, C.A. Inelastic performance of cold-formed steel strap braced walls. *J. Constr. Steel Res.* **2007**, *63*, 460–474. [CrossRef]
5. Balh, N.; DaBreo, J.; Ong-Tone, C.; El-Saloussy, K.; Yu, C.; Rogers, C.A. Design of steel sheathed cold-formed steel framed shear walls. *Thin-Walled Struct.* **2014**, *75*, 76–86. [CrossRef]
6. Shamim, I.; Roger, C.A. Steel sheathed/CFS framed shear walls under dynamic loading: Numerical modelling and calibration. *Thin-Walled Struct.* **2013**, *71*, 57–71. [CrossRef]
7. Zeynalian, M.; Ronagh, H.R. Seismic performance of cold formed steel walls sheathed by fibre-cement board panels. *J. Constr. Steel Res.* **2015**, *107*, 1–11. [CrossRef]
8. Yu, C. Shear resistance of cold-formed steel framed shear walls with 0.686 mm, 0.762 mm, and 0.838 mm steel sheet sheathing. *Eng. Struct.* **2010**, *32*, 1522–1529. [CrossRef]
9. Landolfo, R.; Fiorino, L.; Della Corte, G. Seismic behavior of sheathed cold-formed structures: Physical tests. *J. Struct. Eng.* **2006**, *132*, 570–581. [CrossRef]
10. Fiorino, L.; Della Corte, G.; Landolfo, R. Experimental tests on typical screw connections for cold-formed steel housing. *Eng. Struct.* **2007**, *29*, 1761–1773. [CrossRef]
11. Macillo, V.; Fiorino, L.; Landolfo, R. Seismic response of CFS shear walls sheathed with nailed gypsum panels: Experimental tests. *Thin-Walled Struct.* **2017**, *120*, 161–171. [CrossRef]
12. Fiorino, L.; Shakeel, S.; Macillo, V.; Landolfo, R. Seismic response of CFS shear walls sheathed with nailed gypsum panels: Numerical modelling. *Thin-Walled Struct.* **2018**, *122*, 359–370. [CrossRef]
13. Fiorino, L.; Macillo, V.; Landolfo, R. Shake table tests of a full-scale two-story sheathing-braced cold-formed steel building. *Eng. Struct.* **2017**, *151*, 633–647. [CrossRef]
14. Fiorino, L.; Iuorio, O.; Macillo, V.; Landolfo, R. Performance-based design of sheathed CFS buildings in seismic area. *Thin-Walled Struct.* **2012**, *61*, 248–257. [CrossRef]
15. Kechidi, S.; Bourahla, N. Deteriorating hysteresis model for cold-formed steel shear wall panel based on its physical and mechanical characteristics. *Thin-Walled Struct.* **2016**, *98*, 421–430. [CrossRef]
16. Kechidi, S.; Bourahla, N.; Castro, J.M. Seismic design procedure for cold-formed steel sheathed shear wall frames: Proposal and evaluation. *J. Constr. Steel Res.* **2017**, *128*, 219–232. [CrossRef]
17. Fülop, L.A.; Dubina, D. Design criteria for seam and sheeting-to-framing connections of cold-formed steel shear panels. *J. Struct. Eng.* **2006**, *132*, 582–590. [CrossRef]
18. Dubina, D. Behavior and performance of cold-formed steel-framed houses under seismic action. *J. Constr. Steel Res.* **2008**, *64*, 896–913. [CrossRef]
19. Peterman, K.D.; Stehman, M.J.; Madsen, R.L.; Buonopane, S.G.; Nakata, N.; Schafer, B.W. Experimental seismic responses of a full-scale cold-formed steel-framed building. I: System-level response. *J. Struct. Eng.* **2016**, *142*, 04016127. [CrossRef]
20. Peterman, K.D.; Stehman, M.J.; Madsen, R.L.; Buonopane, S.G.; Nakata, N.; Schafer, B.W. Experimental seismic responses of a full-scale cold-formed steel-framed building. II: Subsystem-level response. *J. Struct. Eng.* **2016**, *142*, 04016128. [CrossRef]
21. Leng, J.Z.; Peterman, K.D.; Bian, G.B.; Buonopane, S.G.; Schafer, B.W. Modeling seismic responses of a full-scale cold-formed steel-framed building. *Eng. Struct.* **2017**, *153*, 146–165. [CrossRef]
22. Smith, B.H.; Arwade, S.R.; Schafer, B.W.; Moen, C.D. Design component and system reliability of a low-rise cold formed steel framed commercial building. *Eng. Struct.* **2016**, *127*, 434–446. [CrossRef]
23. Wang, X.; Pantoli, E.; Hutchinson, T.C.; Restrepo, J.I.; Wood, R.L.; Hoehler, M.S.; Grezesik, P.; Sesma, F.H. Seismic performance of cold-formed steel wall systems in a full-scale building. *J. Struct. Eng. ASCE* **2015**, *141*, 04015014. [CrossRef]

24. Ye, J.H.; Wang, X.X.; Jia, H.Y.; Zhao, M.Y. Cyclic performance of cold-formed steel shear walls sheathed with double-layer wallboards on both sides. *Thin-Walled Struct.* **2015**, *92*, 146–159. [CrossRef]
25. Wang, X.X.; Ye, J.H. Reversed cyclic performance of cold-formed steel shear walls with reinforced end studs. *J. Constr. Steel Res.* **2015**, *113*, 28–42. [CrossRef]
26. Wang, X.X.; Ye, J.H.; Yu, Q. Improved equivalent bracing model for seismic analysis of mid-rise CFS structures. *J. Constr. Steel Res.* **2017**, *136*, 256–264. [CrossRef]
27. Ye, J.H.; Jiang, L.Q.; Wang, X.X. Seismic failure mechanism of reinforced cold-formed steel shear wall based on structural vulnerability analysis. *Appl. Sci.* **2017**, *7*, 182. [CrossRef]
28. Ye, J.H.; Jiang, L.Q. Collapse mechanism analysis of a steel-moment frame based on structural vulnerability theory. *Arch. Civ. Mech. Eng.* **2018**, *18*, 833–843.
29. American Iron and Steel Institute (AISI). *North American Standard of Cold-Formed Steel Framing–Lateral Design*; AISI S400; AISI: Washington, DC, USA, 2015.
30. *Code for Seismic Design of Buildings (GB 50011-2010)*; China Architecture & Building Press: Beijing, China, 2016. (In Chinese)
31. *Technical Specification for Low-Ries Cold-Formed Thin-Walled Steel Buildings (JGJ 227-2011)*; China Environmental Science Press: Beijing, China, 2011. (In Chinese)
32. Pacific Earthquake Engineering Research Center. *Open System for Earthquake Engineering*; Pacific Earthquake Engineering Research Center, University of California: Berkley, CA, USA, 2006.
33. Padilla-Llano, D.A. *A Framework for Cyclic Simulation of Thin-Walled Cold-Formed Steel Members in Structural Systems*; Virginia Polytechnic Institute and State University: Blacksburg, VA, USA, 2015.
34. AISC-LRFD. *Load and Resistance Factor Design Specification for Structural Steel Buildings*; American Institute of Steel Construction: Chicago, IL, USA, 1999.
35. Tao, Z.; Uy, B.; Liao, F.Y.; Han, L.H. Nonlinear analysis of concrete-filled square stainless steel stub columns under axial compression. *J. Constr. Steel Res.* **2011**, *67*, 1719–1732. [CrossRef]
36. Buonopane, S.G.; Bian, G.; Tun, T.H.; Schafer, B.W. Computationally efficient fastener-based models of cold-formed steel shear walls with wood sheathing. *J. Constr. Steel Res.* **2015**, *110*, 137–148. [CrossRef]
37. Ye, J.H.; Chen, W.; Wang, Z. Fire-resistance behavior of a newly developed cold-formed steel composite floor. *J. Struct. Eng.* **2017**, *143*, 04017018. [CrossRef]